Inverse Problems and Imaging

doi:10.3934/ipi.2023047

STABILITY FOR THE INVERSE SOURCE PROBLEM IN A TWO-LAYERED MEDIUM SEPARATED BY ROUGH INTERFACE

Guanghui Hu [1], Xiang Xu [*2], Xiaokai Yuan [3] and Yue Zhao [4]

[1]School of Mathematical Sciences and LPMC, Nankai University, 300071 Tianjin, China

[2]School of Mathematical Sciences, Zhejiang University, Hangzhou 310058, China

[3]School of Mathematics, Jilin University, Changchun, Jilin 130012, China

[4]School of Mathematics and Statistics
Central China Normal University, Wuhan 430079, China

(Communicated by Habib Ammari)

Abstract. In this paper, we investigate an inverse source problem for the two-dimensional Helmholtz equation in a two-layered medium. The interface between two media is assumed to be nonlocal and rough, while the compactly supported unknown source is buried in the lower-half medium. For the forward problem, we prove the radiating behaviour of the wave field based on the Angular Spectrum Representation and the asymptotics of Hankel functions. For the inverse problem, using multi-frequency interface measurements, which are limited-aperture, we show an increasing stability estimate which consists of two parts: one part is a Hölder stability estimate, the other part is a logarithmic stability estimate. The latter decreases as the upper bound of the frequency increases. In the derivation of the stability, we require the source function to have an H^3 regularity to control the high frequency tail of its Fourier transform. To recover the source numerically, we propose a recursive Kaczmarz-Landweber iteration scheme with incomplete data. Numerical examples are presented to justify the theoretical stability estimate and validity of the scheme.

1. **Introduction.** Inverse source scattering problems are encountered in a wide range of scientific and engineering fields, such as antenna design and synthesis, medical imaging, radar technology, and sonar [3, 7, 15]. However, the uniqueness of the inverse problem at a fixed frequency cannot be guaranteed due to non-radiating sources [2, 10]. One solution is to use multi-frequency boundary measurements, which has been shown to restore uniqueness and increase stability in numerical experiments [7, 4]. Recent studies have examined increasing stability for inverse source problems in time-harmonic acoustic, elastic, electromagnetic, and fourth-order plate wave equations [6, 13, 18, 23, 24, 25, 30]. These studies have derived a unified form of increasing stability, demonstrating that higher frequency data leads to greater stability. However, these studies have only considered inverse source

2020 *Mathematics Subject Classification.* Primary: 35R30; Secondary: 78A46.

Key words and phrases. Inverse source problem, two-layered medium, rough interface, stability, Landweber iteration.

*Corresponding author: Xiang Xu.

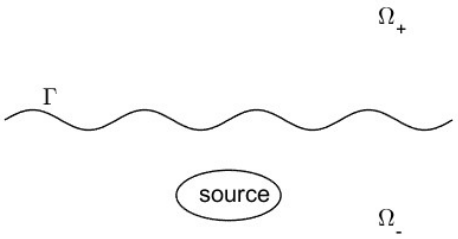

FIGURE 1. Problem geometry

problems in homogeneous or bounded inhomogeneous media. In this paper, we extend this analysis to a two-layered medium with an unbounded rough interface.

Assume the interface between two different media is denote by a rough curve $\Gamma := \{x_2 = g(x_1), x_1 \in \mathbb{R}\}$ in $\mathbb{R}^2$, where g is a bounded Lipschitz function. Denote by Ω_+ (resp. Ω_-) the unbounded domain above (resp. below) Γ. Suppose further that $\Omega_\pm$ are filled with homogeneous and isotropic acoustic material. Set $h = \max_{x_1\in\mathbb{R}} |g(x_1)| < \infty$. Let $\omega > 0$ be the angular frequency. Let $k(x)$ be the wavenumber of the two-layered medium defined by

$$k^2(x) = \begin{cases} k_+^2 = c_+^2\omega^2, & x \in \Omega_+, \\ k_-^2 = c_-^2\omega^2, & x \in \Omega_-, \end{cases}$$

where c_+, c_- are two positive constants with $c_+ \neq c_-$ which are related to the acoustic velocity in the upper and lower half medium, respectively. The propagation of the radiated field u by the source function f is governed by the following Helmholtz equation

$$\triangle u(x,\omega) + k^2(x)u(x,\omega) = f(x), \quad x \in \mathbb{R}^2. \tag{1}$$

Assume that the source function f is located in the lower half medium Ω_- and has compact support such that $\text{supp} f \subset \Omega \subset\subset B_R^-$. Here Ω denotes an open set and $B_R^- := \{x : |x| < R,\ x \in \Omega_-\}$ with radius R. The problem geometry is illustrated in Figure 1.

To ensure the uniqueness of the wave field, we assume that u satisfies the upward and downward Angular Spectrum Representations (ASR) in $\pm x_2 > H$ for all $H > h$:

$$u(x_1,x_2) = \frac{1}{2\pi}\int_{\mathbb{R}} e^{i\sqrt{k_\pm^2-\xi^2}(x_2\mp H)+ix_1\xi}\mathcal{F}u(\xi,\pm H)\,d\xi, \quad \pm x_2 \geq H, \tag{2}$$

where $\mathcal{F}v(\xi)$ denotes the Fourier transform of v on $\mathbb{R}$ defined by

$$\mathcal{F}(v)(\xi) = \int_{\mathbb{R}} v(x_1)e^{-\mathrm{i}\xi x_1}\mathrm{d}x_1,$$

and the corresponding inverse Fourier transform is defined by

$$\mathcal{F}^{-1}(v)(x_1) = \frac{1}{2\pi}\int_{\mathbb{R}} v(\xi)e^{\mathrm{i}\xi x_1}\mathrm{d}\xi.$$

The above formulation (1)-(2) also models the TE polarization for electromagnetic radiating problems. Using variational approach in weighted Sobolev spaces,

one can prove that the source radiating problem (1)-(2) admits a unique solution in the space

$$H^1_\rho(W_H) = \{u \in H^1(W_H) : (1 + x_1^2)^{\rho/2} u \in H^1(W_H)\} \quad \text{for all} \quad H > h, |\rho| < 1.$$

Here $W_H := \{x \in \mathbb{R}^2 : |x_2| \leq H\}$ denotes a strip with the height $H > 0$. The Angular Spectral Representation (2) was firstly used in [11] as a formal radiation condition for rough surface scattering problems, making it possible to analyze an equivalent variational formulation posed in the unbounded strip W_H through transparent boundary operators defined on $x_2 = \pm H$. The uniqueness proof follows from the use of Rellich identities for smooth interfaces given by some graph. We refer to [12] for the proof of well-posedness in weighted Sobolev spaces under the Dirichelt boundary condition and to [16, 27] with general transmission conditions.

In this paper, the focus is on determining the unknown function f from multi-frequency interface measurements $\{u(x,\omega)|_\Gamma, \partial_\nu u(x,\omega)|_\Gamma\}$ with ω being given in a finite interval. Previous research has been done on the uniqueness and numerical methods for recovering penetrable or impenetrable inhomogeneities in a two-layered medium [5, 21, 22, 26, 28], and more recently, increasing stability for the inverse source problem in a multi-layered medium in one dimension was studied [29]. Compared to the one-dimensional case, the analysis for two-dimensional case has two additional difficulties. One is that the interface is unbounded and rough. The other is that the radiating field can be only measured on the interface for practical applications, which means the observation data is limited aperture. These two difficulties prevent direct extension of existing methods on obtaining an increasing stability.

Generally speaking, increasing stability analysis mainly consists of two steps. The first step is to bridge the unknown source function and boundary measurements. There are commonly two methods for this, including transforming the frequency-domain inverse source problem to the identification of the initial value of the corresponding time-domain wave equation by Fourier transform (see e.g. [13]), or directly multiplying the elliptic equation by either plane waves or eigenfunctions and integrating by parts (see e.g. [23, 25]). However, these methods typically require measurements on the entire boundary of a bounded domain enclosing the support of the source function. This is not feasible in a two-layered medium since the measurements are only taken on the unbounded interface. To address this limitation, the fundamental solution in free space is taken as the test function, and its asymptotic behavior is utilized to relate the Fourier transform of the source function to the boundary measurements on the interface. The validity of this approach is justified mathematically by well-posed results from other studies [16, 17]. The second step involves the analytic continuation principle. However, due to our limited ability to measure the source function on the interface, some information is lost in comparison to previous inverse source problems studied in [13, 23]. Specifically, we may only have access to observation directions in the upper-half unit circle. This limitation is reflected mathematically in Lemma 3.1, which shows that only a portion of the Fourier transform of the source function can be recovered through our limited-aperture measurements. To overcome this challenge and recover the missing frequency components of the Fourier transform, we employ a quantitative analytic continuation result presented in [1]. Ultimately, by applying the argument of analytic continuation, we are able to establish increasing stability. The stability estimate is determined by considering two factors: the Hölder-type data discrepancy and a logarithmic-type stability estimate. Notably, as the frequency of the observed

data increases, the contribution of the high frequency tail decreases. Consequently, the inverse problem becomes more stable when higher frequency data is utilized. Thus, collecting data with greater frequency will lead to a more robust inversion process in practice. In the derivation of the stability, we require the source function to have an H^3 regularity. In general, to obtain increasing stability estimates in inverse scattering problems, regularity assumptions are necessary to control the high frequency tail of the Fourier transforms of the unknown functions.

This paper is organized as follows. In Section 2 we study the radiating behavior of the solution to the direct scattering problem. Section 3 is devoted to the stability analysis of the inverse source problem by multi-frequency boundary measurements on the interface. In Section 4 we present several numerical examples to justify the theoretical increasing stability estimate.

2. Radiating behavior of wave field.

In this section we shall study the radiating behavior of u to the direct source scattering problem (1)–(2) in the radial directions. Set $C_a := \{x \in \mathbb{R}^2 : |x| = a\}$ for $a > 0$ and $U_{\pm b} = \{x : \pm x_2 > b\}$. Define the weighted Sobolev spaces $H^s_\rho(\mathbb{R}) := (1+x^2)^{-\rho/2} H^s(\mathbb{R})$ for $\rho, s \in \mathbb{R}$.

Theorem 2.1. *The unique solution u to (1)-(2) fulfills the following relations*

$$\begin{aligned} &\sup_{x\in C_a\cap U_{\pm H}} |x|^{1/2} \left| \frac{\partial u(x)}{\partial r} - ik_\pm u(x) \right| \;\to\; 0\,, \quad a\to\infty\,, \quad r=|x|, \\ &\sup_{x\in U_{\pm H}} |x|^{1/2}|u(x)| \;<\; \infty, \end{aligned} \tag{3}$$

for all $H > h$.

Proof. It is essential to verify that the functions given by Angular Spectrum Representation (2) satisfies the asymptotics in (3), provided the function $x_1 \mapsto u(x_1, \pm H) \in H^{1/2}_\rho(\mathbb{R})$ for all $H > h$ and $\rho \in (1/2, 1)$. This was firstly proved in [17, Appendix, Lemma A.2]. Below we present a simplified version by refining the arguments in [17, Appendix] and [20, Section 6].

Without loss of generality we suppose $g(x_1) < 0$ and only consider the upper half space $U_0 = \mathbb{R}^2_+ = \{x : x_2 > 0\}$. Note that the upward ASR (2) is equivalent to the following Upward Propagating Radiation Condition (UPRC):

$$u(x) = 2\int_{y_2=0} \frac{\partial \Phi(x;y)}{\partial y_2}\, u(y)\, ds(y), \qquad x_2 > 0. \tag{4}$$

Here $\Phi(x,y) := \frac{i}{4} H_0^{(1)}(k_+|x-y|)$ denotes the free-space fundamental solution to the two-dimensional Helmholtz equation.

Using the fact that $u(x_1, 0) \in L^2_\rho(\mathbb{R})$ with $\rho > 1/2$ and the asymptotics of Hankel functions for large arguments, we have for $x_2 > 0$ that

$$\begin{aligned} |u(x_1,x_2)| &\le Cx_2 \int_{y_2=0} \frac{1}{|x-y|^{3/2}} |u(y)|\, ds(y) \\ &\le Cx_2 \int_{\mathbb{R}} \frac{1}{(|x_1-y_1|^2+x_2^2|)^{3/4}} \frac{1}{1+|y_1|^{3/2}}\, dy_1 \\ &\le Cx_2 \int_{|y_1|>1} \frac{1}{(|x_1-y_1|^2+x_2^2|)^{3/4}} \frac{1}{|y_1|^{3/2}}\, dy_1, \end{aligned}$$

where $C > 0$ is independent of x. Recalling [17, Lemma 4.1] with $n = \rho = 3/4$ (see also [20, Lemma 2.5] with $q = \rho = 3/4$), we obtain the upper bound

$$|u(x_1, x_2)| \quad \leq \quad \begin{cases} C\,|x_2|^{-1/2} & \text{if} \quad |x_1| < |x_2|, \\ C\,(|x_2|\,|x_1|^{-3/2} + |x_1|^{-3/4}) & \text{if} \quad |x_1| \geq |x_2|, \end{cases}$$

which leads to the estimate

$$\sqrt{r}\,|u(x_1, x_2)| < C, \qquad \text{uniformly for all} \quad x \in \mathbb{R}^2_+, \quad r = |x|. \tag{5}$$

This proves the second estimate in (3). Moreover, the estimate in (5) implies that, for any $\epsilon > 0$,

$$A_M(x) := \sqrt{r} x_2 \int_{|y_1|>M} \frac{1}{(|x_1 - y_1|^2 + x_2^2|)^{3/4}} \frac{1}{|y_1|^{3/2}}\, dy_1 < \epsilon/2, \tag{6}$$

uniformly holds for all $x \in \mathbb{R}^2_+$, provided $M = M(\epsilon) > 0$ is chosen to be sufficiently large.

To prove the first estimate of u in (3), we split the integral for $\partial_r u - iku$ into two parts:

$$\begin{aligned} \partial_r u - iku \quad &= \quad \left(\int_{|y_1|<M} + \int_{\{|y_1|>M\}} \right) (\partial_r - ik)\, \frac{\partial \Phi(x; 0, y_2)}{\partial y_2}\, u(y_1, 0) \mathrm{d}y_1 \\ &:= \quad I_1(x) + I_2(x), \end{aligned} \tag{7}$$

with the second one bounded by (see [17, Formula (4.14), (4.15)])

$$|I_2(x)| \leq C \int_{\{|y_1|>M, y_2=0\}} \frac{x_2}{|x - y|^{3/2}} \left| \frac{|x - y| - |x| + \hat{x} \cdot y}{|x - y|} \right| \frac{1}{|y_1|^{3/2}}\, \mathrm{d}y_1. \tag{8}$$

Combining (6) and the fact that

$$\left| \frac{|x - y| - |x| + \hat{x} \cdot y}{|x - y|} \right| < 1 \quad \text{for all} \quad x \in \mathbb{R}^2_+, \quad y_2 = 0, \tag{9}$$

we can further estimate I_2 by

$$\sqrt{r}\,|I_2(x)| \leq |A_M(x)| \leq \epsilon/2. \tag{10}$$

On the other hand, since the integral for I_1 is restricted to a compact set, we have

$$|\sqrt{r}\, I_1(x)| = \left| \sqrt{r}(\partial_r - ik) \int_{\{|y_1|<M, y_2=0\}} \frac{\partial \Phi(x; y)}{\partial y_2}\, u(y)\, ds(y) \right| < \epsilon/2, \tag{11}$$

for $r > 0$ sufficiently large depending only on $\epsilon > 0$. Finally, combining (7), (10) and (11) we obtain

$$|\sqrt{r}\,(\partial_r u - iku)| \leq \sqrt{r}\,|I_1(x) + I_2(x)| < \epsilon, \tag{12}$$

provided $r = r(\epsilon) > 0$ is sufficiently large. This together with (5) proves the estimates in (3). □

Remark 2.2. Along the horizontal directions in the strip W_H with $H > h$, there holds the asymptotics

$$|u(x)|, |\nabla u(x)| = O(|x_1|^{-3/2}) \quad \text{as} \quad |x| \to \infty \quad \text{in} \quad W_H. \tag{13}$$

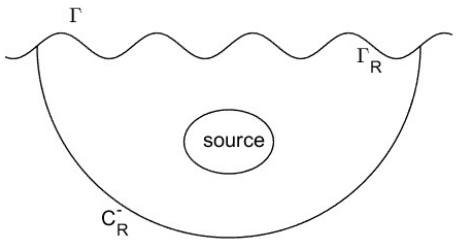

FIGURE 2. Integration domain

3. **Stability estimate.** In this section, the main result for the inverse source problem is derived. As mentioned in the introduction, the procedure consists of two steps which are given by Lemma 3.1 and Lemma 3.3 respectively.

Denote the Fourier transform of f in $\mathbb{R}^2$ by $\hat{f}(\xi) = \int_{\mathbb{R}^2} f(y)e^{-\mathrm{i}y\cdot\xi}\mathrm{d}y$, and the upper-half unit circle by $\mathbb{S}^+$. The following lemma bridges the unknown source function f with the interface measurements $\{u(x,\omega)|_\Gamma, \partial_\nu u(x,\omega)|_\Gamma\}$ on Γ.

Lemma 3.1. *For $\theta = (\theta_1, \theta_2) \in \mathbb{S}^+$ one has*

$$\hat{f}(k_-\theta) = \int_\Gamma \left[\partial_\nu u(y)e^{-\mathrm{i}k_-\theta\cdot y} + ik_-\left(\nu(y)\cdot\theta\right)e^{-\mathrm{i}k_-\theta\cdot y}u(y)\right]\,\mathrm{d}s(y).$$

Proof. For $z \in \mathbb{R}^2_+$ denote $\hat{z} = \frac{z}{|z|} = (\hat{z}_1, \hat{z}_2) \in \mathbb{S}^+$. Denote $\partial B_R^- = \Gamma_R \cup C_R^-$ where $\Gamma_R = \{y \in \Gamma : |y| \le R\}$ and $C_R^- = \{y : |y| = R, y \in \Omega_-\}$. Multiplying both sides of the equation (1) by the two-dimensional fundamental solution $G^i(z,y) = \frac{\mathrm{i}}{4}H_0^{(1)}(k_-|z-y|)$ corresponding to the wavenumber k_- in free space and integrating by parts over B_R^- yield

$$\begin{aligned}\int_\Omega f(y)G^i(z,y)dy = &\int_{\Gamma_R} \partial_\nu u(y)G^i(z,y) - \partial_\nu G^i(z,y)u(y)\mathrm{d}s(y)\\ &+ \int_{C_R^-\cap W_H} \partial_\nu u(y)G^i(z,y) - \partial_\nu G^i(z,y)u(y)\mathrm{d}s(y)\\ &+ \int_{C_R^-\cap\{x_2<-H\}} \partial_\nu u(y)G^i(z,y) - \partial_\nu G^i(z,y)u(y)\mathrm{d}s(y)\end{aligned}$$

where $R > H > h$. Here we have supposed that the domain B_R^- is a Lipschitz domain by the choice of $R > 0$. The integration domain is illustrated in Figure 2.

Since both $G^i(z,y)$ and u satisfy the Sommerfeld radiation condition (2), letting $R \to \infty$ one obtains that

$$\lim_{R\to\infty}\int_{C_R^-\cap\{x_2<-H\}} \partial_\nu u(y)G^i(z,y) - \partial_\nu G^i(z,y)u(y)\mathrm{d}s(y) = 0.$$

The asymptotics of u in horizontal directions (see Remark 2.2) yield that

$$\lim_{R\to\infty}\int_{C_R^-\cap W_H} \partial_\nu u(y)G^i(z,y) - \partial_\nu G^i(z,y)u(y)\mathrm{d}s(y) = 0.$$

Hence, letting $R \to \infty$ one deduces

$$\int_\Omega f(y)G^i(z,y)dy = \int_\Gamma \partial_\nu u(y)G^i(z,y) - \partial_\nu G^i(z,y)u(y)\mathrm{d}s(y).$$

Now, we recall the asymptotic behavior of $H_0^{(1)}(t)$ in [14]

$$H_0^{(1)}(t) = \frac{\sqrt{2}}{\sqrt{\pi t}} e^{\mathrm{i}(t-\pi/4)}\Big(1 + O\Big(\frac{1}{t}\Big)\Big)$$

and

$$|z-y| = \sqrt{|z^2| - 2z\cdot y + |y|} = |z| - \hat{z}\cdot y + \mathcal{O}\Big(\frac{1}{|z|}\Big).$$

Fixing $\hat{z} \in \mathbb{S}^+$ and letting $|z| \to \infty$ we derive

$$\hat{f}(k_-\hat{z}) = \int_\Omega f(y)e^{-\mathrm{i}k_-\hat{z}\cdot y}\mathrm{d}y = \int_\Gamma \partial_\nu u(y)e^{-\mathrm{i}k_-\hat{z}\cdot y} - \Big(\partial_\nu e^{-\mathrm{i}k_-\hat{z}\cdot y}\Big)u(y)\mathrm{d}s(y).$$

Note that the function $y \mapsto e^{-ik_-\hat{z}\cdot y}$ belongs to the weighted Sobolev space $H^1_\rho(W_H)$ with $\rho < -1/2$, the first integral over Γ is understood as the dual form between $H^{-1/2}_\rho$ and $H^{1/2}_{-\rho}$ with $\rho \in (1/2,1)$, while the second one between $H^{1/2}_\rho$ and $H^{-1/2}_{-\rho}$ with $\rho \in (1/2,1)$. By the arbitrariness of $z \in \mathbb{R}^2_+$ and letting $\theta = \hat{z}$ the proof is completed. □

Remark 3.2. In the special case that $\Gamma = \{x_2 = 0\}$ is flat, we have

$$\int_\Omega f(y)e^{-\mathrm{i}k_-\hat{z}\cdot y}\mathrm{d}y = \int_\Gamma \left[\partial_{y_2}u(y)e^{-\mathrm{i}k_-\hat{z}_1 y_1} + \mathrm{i}k_-\hat{z}_2 e^{-\mathrm{i}k_-\hat{z}_1 y_1}u(y)\right]\mathrm{d}s(y),$$

which gives

$$\hat{f}(k_-\hat{z}) = \mathcal{F}(\partial_{y_2}u)(k_-\hat{z}_1) + \mathrm{i}k_-\hat{z}_2\mathcal{F}(u)(k_-\hat{z}_1).$$

Next we proceed to the second step of analytic continuation principle. The proof is similar as [1, Lemma 2.2] and omitted here. Hereafter, the notation $a \lesssim b$ stands for $a \le Cb$, where $C > 0$ is a generic constant which may change step by step in the proofs.

Lemma 3.3. *Let $v \in L^2(\mathbb{R}^2)$ with compact support. Then there exists an $\alpha \in (0,1)$ such that*

$$\|\hat{v}\|_{L^\infty(B_K)} \lesssim e^{K(1-\alpha)}\|\hat{v}\|^\alpha_{L^\infty(B_K^+)}.$$

Here $B_K = \{\xi : |\xi| \le K\}$ and $B_K^+ = \{\xi : |\xi| \le K, \xi_2 \ge 0\}$.

Now we are in the position to discuss the inverse problem, i.e., to determine an unknown source f from the data $\{u(x,\omega)|_\Gamma, \partial_\nu u(x,\omega)|_\Gamma\}$ measured on the interface Γ for $\omega \in (0,K)$. Assume $f \in \mathcal{C}_M$ which is a real-valued functional space defined by

$$\mathcal{C}_M = \{f \in H^n(\mathbb{R}^2) : \|f\|_{H^n(\mathbb{R}^2)} \le M, \mathrm{supp} f \subset \Omega, f : \Omega \to \mathbb{R}, n \ge 3\}.$$

Moreover, let the data collected on the interface be characterized by ϵ

$$\epsilon := \sup_{|\xi|\le c_- K} \Big| \int_\Gamma \left[\partial_\nu u(y)e^{-\mathrm{i}\xi\cdot y} + i\left(\nu(y)\cdot\xi\right)e^{-\mathrm{i}\xi\cdot y}u(y)\right]\mathrm{d}s(y)\Big|. \tag{14}$$

For the special case when $\Gamma = \{x_2 = 0\}$, the observation data can be simplified as

$$\epsilon := \sup_{|\xi|\le c_- K} \Big(|\mathcal{F}(\partial_{x_2}u)(\xi)| + K|\mathcal{F}(u)(\xi)|\Big).$$

Theorem 3.4. *Let $u(x,\omega)$ be the solution of the scattering problem (1)-(2) with the source $f \in \mathcal{C}_M$. Then*

$$\|f\|^2_{L^2(\Omega)} \lesssim e^{2(1-\alpha)K}\epsilon^{2\alpha} + \frac{M^2}{K^{\gamma_1}|\ln\epsilon|^{\gamma_2}}, \tag{15}$$

where $\alpha \in (0,1)$ is a positive constant specified in Lemma 3.3, $\gamma_1 = \frac{4n-10}{3}, \gamma_2 = \frac{2n-5}{4}$.

Proof. Assume ϵ is small, otherwise the estimate is obvious. For $s \in \mathbb{C}$ denote

$$I(s) = \int_0^s k \int_{\mathbb{S}} \hat{f}(k\theta)\hat{f}(-k\theta)\mathrm{d}\theta\mathrm{d}k,$$

where the integral is taken over the line segment joining the origin and s in the complex plane. Then $I(s)$ is analytic for $s \in \mathbb{C}$. Noticing $\overline{\hat{f}(k\theta)} = \hat{f}(-k\theta)$ when k and f are real, one has that for $K > 0$

$$\tilde{\epsilon}^2 := I(K) = \int_{|\xi|\le K} |\hat{f}(\xi)|^2 \mathrm{d}\xi.$$

Applying the argument of analytic continuation as the proof of [23, Theorem 2.1] one obtains that

$$\|f\|^2_{L^2(\Omega)} \lesssim \tilde{\epsilon}^2 + \frac{M^2}{K^{\gamma_1}|\ln\tilde{\epsilon}|^{\gamma_2}}, \tag{16}$$

where $\gamma_1 = \frac{4n-10}{3}, \gamma_2 = \frac{2n-5}{4}$.

Next, using the analytic continuation principle in Lemma 3.3 one has that

$$\tilde{\epsilon}^2 = I(K) \lesssim K^2\|\hat{f}\|^2_{L^\infty(B_K)} \lesssim K^2 e^{2(1-\alpha)K}\|\hat{f}\|^{2\alpha}_{L^\infty(B_K^+)} \lesssim K^2 e^{2(1-\alpha)K}\epsilon^{2\alpha}, \tag{17}$$

where in the last inequality we have used the following estimate which is a direct consequence of Lemma 3.1:

$$\|\hat{f}\|_{L^\infty(B_K^+)} \lesssim \epsilon.$$

Thus, replacing $\tilde{\epsilon}$ in (16) by the right hand side of (17) we complete the proof. □

Note that the stability estimate in free space [23] consists of a Lipschitz type data discrepancy other than the Hölder one appearing in the current case. Moreover, one does not have the exponential upper bound in (15) for the case of free space. The reason is that the inverse source problem considered in this paper only assumes the limited-aperture measurements on the interface. As a consequence, to recover the unseen part of the unknown source function the application of the analytic continuation principle in Lemma 3.3 seems to be inevitable, which leads to the appearance of the data discrepancy of Hölder type as well as the exponential upper bound.

4. Numerical experiments.

In this section, we present some numerical examples to demonstrate the increasing stability with multiple frequencies for the special case when the interface $\Gamma = \{x_2 = 0\}$ is flat. For the flat interface, we can use the explicit Green's function to generate the scattered field. In comparison, for general rough surfaces, we may have to compute the outgoing waves by other methods such as using the perfectly matched layer. In this case, the cost of the computation is usually high. We leave the numerics for general rough surfaces for future work. We would like to mention that flat interfaces also arise in many practical applications.

In general, the increased stability could be considered as an intrinsic nature of inverse problems, which shows that the stability improves as more frequencies of data are used. This phenomenon has been observed numerically in e.g. [4]. In this manuscript, we derive (15) to verify the increased stability estimate for the inverse source scattering problem from a mathematical point of view. Then we further verify (15) numerically in Section 4. Thus, (15) itself may not provide a numerical method directly. It is intended to reveal the phenomenon of increased stability mathematically.

For the flat interface, the Green's function for a two-layered medium where the fixed source point y is located in the lower-half plane $\mathbb{R}^2_- := \{y : y_2 < 0\}$ takes the explicit form [21]

$$G(x,y) = \begin{cases} G^t(x,y), & x_2 > 0, \\ G^i(x,y) + G^r(x,y), & x_2 < 0, \end{cases}$$

where

$$\begin{aligned} G^i(x,y) &= \frac{\mathrm{i}}{4} H_0^{(1)}(k_-|x-y|), \\ G^t(x,y) &= \frac{\mathrm{i}}{2\pi} \int_{\mathbb{R}} \frac{e^{\mathrm{i}(\beta_1 x_2 - \beta_2 y_2)}}{\beta_1 + \beta_2} e^{\mathrm{i}\eta(x_1-y_1)} \mathrm{d}\eta, \\ G^r(x,y) &= \frac{\mathrm{i}}{4\pi} \int_{\mathbb{R}} \frac{\beta_2 - \beta_1}{\beta_2(\beta_1+\beta_2)} e^{-i\beta_2(x_2+y_2)} e^{\mathrm{i}\eta(x_1-y_1)} \mathrm{d}\eta, \end{aligned}$$

with

$$\beta_1 = \sqrt{k_+^2 - \eta^2}, \quad \beta_2 = \sqrt{k_-^2 - \eta^2}.$$

For fixed $y \in \mathbb{R}^2_-$, the Green's function satisfies

$$-\Delta_x G - k^2 G = \delta(x-y), \quad x \in \mathbb{R}^2,$$

and the following continuation conditions on the interface Γ

$$G^i + G^r = G^t, \quad \partial_{x_2}(G^i + G^r) = \partial_{x_2} G^t.$$

Using the Green's function the solution u to the scattering problem (1)–(2) can be represented by

$$u(x) = \int_{\mathbb{R}^2} G(x,y) f(y) \mathrm{d}y, \quad x \in \mathbb{R}^2. \tag{18}$$

The adopted recovery algorithm is the recursive Kaczmarz-Landweber iteration method [8, 9, 18] outlined in Table 1 below. The algorithm has two level iterations. The outer Kaczmarz iteration starting from the low frequency to high frequency can avoid the local minimum and improve the recovery resolution. The inner Landweber iteration at each frequency treats the ill-posedness of the inverse source problem, which provides a stable reconstruction of the source function. And at each frequency, the final result of the inner Landweber iteration acts as the initial guess for the outer Kaczmarz iteration at next frequency.

To apply the Landweber iteration [19], we need the following two associate measurement operators using (18):

$$\begin{aligned} u(x_1, 0, \omega) := L^1_\omega f(x) &= \frac{\mathrm{i}}{2\pi(k_-^2 - k_+^2)} \\ &\times \int_{\mathbb{R}^2} f(y) \int_{\mathbb{R}} e^{-\mathrm{i}\sqrt{k_-^2 - \eta^2} y_2} \Big(\sqrt{k_-^2 - \eta^2} - \sqrt{k_+^2 - \eta^2} \Big) e^{\mathrm{i}\eta(x_1 - y_1)} \mathrm{d}\eta \mathrm{d}y. \end{aligned}$$

TABLE 1. The recursive Kaczmarz-Landweber iteration method for the inverse source problem.

1. Set the initial guess $f_{2N}^0 = 0$.
2. For $k = 1, 2, ..., K$ (Outer Kaczmarz iteration)
3. $\omega = k$; $f_0^k = f_{2N}^{k-1}$;
4. For $n = 1, 2, ..., N$ (Landweber iteration for Dirichlet measurement)
5. $f_n^k = f_{n-1}^k + \mu \left(L_\omega^1\right)^* \left[u_\omega - L_\omega^1 f_{n-1}^k\right]$.
6. End
7. For $n = N+1, N+2, ..., 2N$ (Landweber iteration for Neumann measurement)
8. $f_n^k = f_{n-1}^k + \mu \left(L_\omega^2\right)^* \left[\partial_{x_2} u_\omega - L_\omega^2 f_{n-1}^k\right]$.
9. End
10. End

$$\partial_{x_2} u(x_1, 0, \omega) := L_\omega^2 f(x) = -\frac{1}{2\pi(k_-^2 - k_+^2)} \times \int_{\mathbb{R}^2} f(y) \int_{\mathbb{R}} e^{-\mathrm{i}\sqrt{k_-^2 - \eta^2} y_2} \left(\sqrt{k_-^2 - \eta^2} - \sqrt{k_+^2 - \eta^2}\right) \sqrt{k_+^2 - \eta^2} e^{\mathrm{i}\eta(x_1 - y_1)} \mathrm{d}\eta \mathrm{d}y.$$

and their adjoint operators $\left(L_\omega^1\right)^*, \left(L_\omega^2\right)^*$. The scaling constant μ in the Landweber iteration is taken in the interval $\left(0, \min\left(\|L_\omega^1\|^{-2}, \|L_\omega^2\|^{-2}\right)\right)$ to guarantee the convergence at each frequency.

In the following examples, we set the positive constants in the wavenumber by $c_1 = 1$ and $c_2 = 2.1$, respectively. The source function f is chosen as

$$\begin{aligned} f(x, y) = {} & 3.1 e^{-200\left((x-0.11)^2 + (y+0.2)^2\right)} + 2.5 e^{-180\left((x+0.11)^2 + (y+0.21)^2\right)} \\ & + 3.1 e^{-180\left((x+0.2)^2 + (y+0.23)^2\right)} + 1.8 e^{-220\left((x-0.15)^2 + (y+0.25)^2\right)} \\ & + 2.7 e^{-240\left((x-0.2)^2 + (y+0.3)^2\right)}, \end{aligned}$$

which is supported in a bounded domain $[-0.5, 0.5] \times [-0.5, 0]$. In our examples, the source function is recovered under the equally discretized mesh with meshsize $h = 0.03$. The measurement data $(u_{\omega_k}, \partial_\nu u_{\omega_k})$ generated by finite element method with PML truncation is collected on the interface Γ with multiple frequencies $\omega_k = k, k = 1, ..., 50$. The interface Γ is unbounded. However, in practice, the measurement data can only be collected in a finite interval. As shown in Remark 2.2, the Cauchy data decay sufficiently fast with respect to x_1:

$$|u(x_1, 0)|, |\partial_{x_2} u(x_1, 0)| = \mathcal{O}(|x_1|^{-3/2}) \quad as\ |x_1| \to \infty.$$

In the first example, we collect the data in a relatively wide interval [-50, 50] so that the Cauchy data beyond this interval is negligible; As a comparison, in the second example, we test the robustness of the proposed method by collecting the measurement data in a relative narrow interval [-5, 5]. Through these two examples, we show that even with a limited measurement data, the reconstruction with multiple frequencies is reliable.

4.1. **Fine measurement on the interval [-50, 50].** In this example, measurement data was collected equally within the range of [-50, 50] with a spacing of $h = 0.03$. On the left and right sides of Figure 3, we present the exact and reconstructed source function, respectively. In order to demonstrate the decrease of

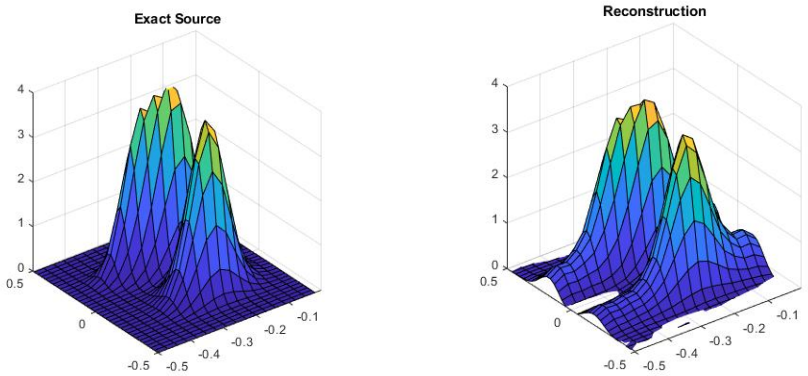

FIGURE 3. Left: exact source; Right: reconstruction

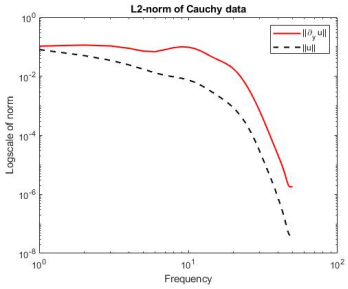

FIGURE 4. L_2-norm of Cauchy data

relative error with respect to frequency, we have displayed the logarithmically-scaled relative error on the left side of Figure 5. It is worth noting that the relative error continues to decrease until $\omega = 27$, after which the quality of reconstruction does not improve. This is due to the fact that the norm of Cauchy data decays as the frequency increases. We have illustrated this phenomenon in Figure 4, which clearly shows that when the frequency is sufficiently large, the Cauchy data on Γ becomes negligible and cannot provide additional information for reconstruction.

In order to showcase the advantages of increased stability with multiple frequencies, we have displayed the relative error at $\omega = 27$ with respect to iteration number on the right side of Figure 5. We observe that the reconstruction stops at a local minimum.

Furthermore, to demonstrate the robustness of our proposed method, we have tested the algorithm with contaminated data having a noise level of 20%. The reconstruction and logarithmically-scaled relative error with respect to frequency are shown in Figure 6. And the relative error at some frequencies is list in Table 2. It is worth noting that even with the presence of noisy data, the reconstruction remains reliable.

4.2. **Coarse measurement on the interval [-5, 5].** In this example, we have tested the robustness of our method with coarse measurements in a narrow interval. Specifically, the measurement data was collected equally within the range of

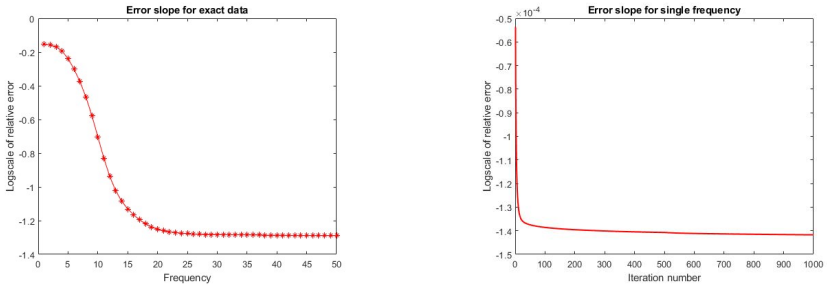

FIGURE 5. Left: error slope with multiple frequencies; Right: error slope with single frequency

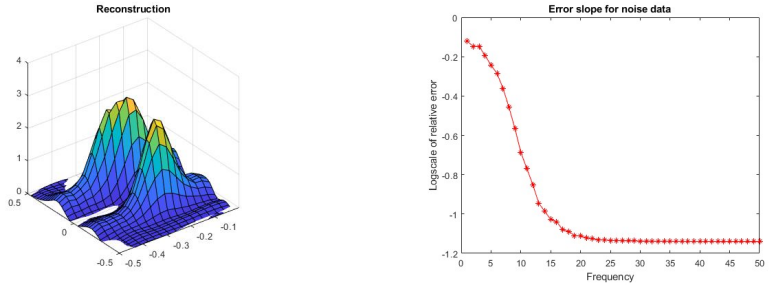

FIGURE 6. Left: reconstruction with 20% noise; Right: error slope with multiple frequencies

TABLE 2. Relative error with fine measurement on [-50, 50]

	$\kappa = 1$	$\kappa = 10$	$\kappa = 20$	$\kappa = 30$	$\kappa = 40$	$\kappa = 50$
Noiseless	0.8571	0.4949	0.2861	0.2774	0.2763	0.2757
20% noise	0.8856	0.5033	0.3290	0.3207	0.3201	0.3198

TABLE 3. Relative error with coarse measurement on [-5, 5]

	$\kappa = 1$	$\kappa = 10$	$\kappa = 20$	$\kappa = 30$	$\kappa = 40$	$\kappa = 50$
Noiseless	0.8633	0.5393	0.3867	0.3830	0.3826	0.3824
20% noise	0.9160	0.6150	0.4699	0.4663	0.4657	0.4654

$[-5, 5]$ with a spacing of $h = 0.5$. The reconstructed source function with multiple frequencies is displayed in Figure 7, where the reconstruction with and without noise is presented on the left and right sides of the figure, respectively. It is evident that even with limited or contaminated data, the reconstruction with multiple frequencies remains reliable. Furthermore, in Figure 8, we have plotted the logarithmically-scaled relative error with respect to frequency. The relative error at some frequencies is list in Table 3. As in the previous example, the relative error decays as the frequency increases until it reaches $\omega = 27$.

5. **Conclusion.** This paper contributes to the understanding and solution of the inverse source problem in a challenging medium with nonlocal and rough interfaces. Theoretical results on the increasing stability using multi-frequency interface measurements are derived and an effective numerical method for source recovery with

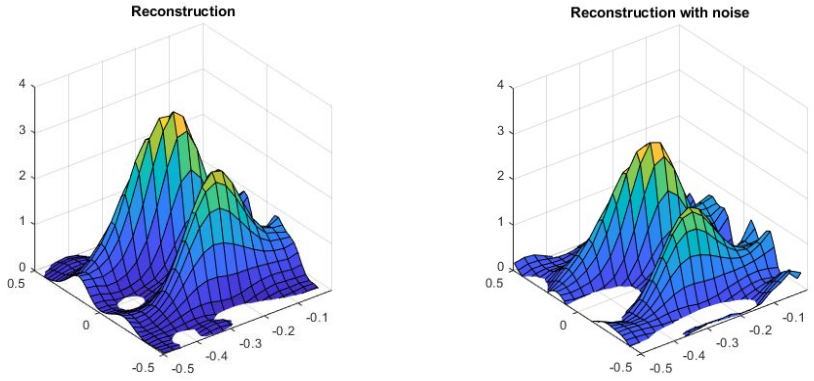

FIGURE 7. Left: reconstruction without noise; Right: reconstruction with 20% noise

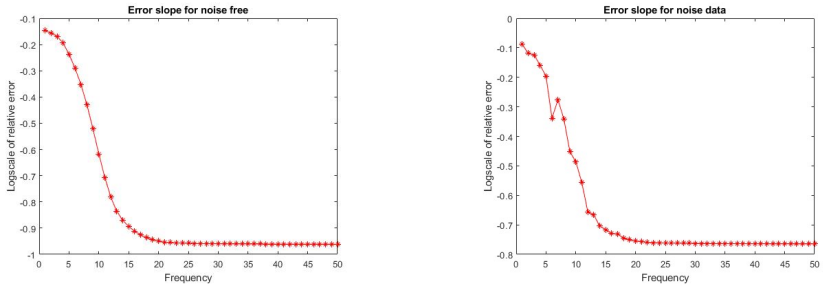

FIGURE 8. Left: error slope without noise; Right: error slope with 20% noise

limited-aperture data is proposed. In future work, it would be interesting to extend the methods to consider the case of multi-layered media or to investigate the inverse source problem in more general settings where the interfaces may be highly irregular and no explicit Green's functions are available. Additionally, developing new techniques for handling incomplete data or exploring alternative regularization strategies could also be fruitful avenues for future research.

Acknowledgments. The authors would like to thank the anonymous reviewers for their insightful suggestions. The research of G. Hu is supported in part by NSFC (No. 12071236) and the Fundamental Research Funds for Central Universities in China (No. 63213025); the research of X. Xu is supported in part by NSFC (No.11621101, No.12071430) and Key Laboratory of Collaborative Sensing and Autonomous Unmanned Systems of Zhejiang Province; the research of X. Yuan is supported in part by NSFC (No.12201245, N0.12171017); the research of Y. Zhao is supported in part by NSFC (No.12001222).

REFERENCES

[1] I. Aicha and G. Hu, An increasing stability estimate for an inverse source problem for the Helmholtz equation, preprint.

[2] R. Albanese and P. B. Monk, The inverse source problem for Maxwell's equations, *Inverse Problems*, **22** (2006), 1023-1035.
[3] C. A. Balanis, *Antenna Theory: Analysis and Design*, Wiley, Hoboken, NJ, 2005.
[4] G. Bao, P. Li, J. Lin and F. Triki, Inverse scattering problems with multi-frequencies, *Inverse Problems*, **31** (2015), 093001, 21 pp.
[5] G. Bao, H. Liu, P. Li and L. Zhang, Inverse obstacle scattering in an unbounded structure, *Commun. Comput. Phys.*, **26** (2019), 1274-1306.
[6] G. Bao, P. Li and Y. Zhao, Stability for the inverse source problems in elastic and electromagnetic waves, *J. Math. Pures Appl.*, **134** (2020), 122-178.
[7] G. Bao, J. Lin and F. Triki, A multi-frequency inverse source problem, *J. Differential Equations*, **249** (2010), 3443-3465.
[8] G. Bao, J. Lin and F. Triki, Numerical solution of the inverse source problem for the Helmholtz equation with multiple frequency data, *Comtemp. Math.*, **548** (2011), 45-60.
[9] G. Bao, S. Lu, W. Rundell and B. Xu, A recursive algorithm for multifrequency acoustic inverse source problems, *SIAM J. Numer. Anal.*, **53** (2015), 1608-1628.
[10] N. Bleistein and J. K. Cohen, Nonuniqueness in the inverse source problem in acoustics and electromagnetics, *J. Math. Phys.*, **18** (1977), 194-201.
[11] S. N. Chandler-Wilde and P. Monk. Existence, uniqueness and variational methods for scattering by unbounded rough surfaces, *SIAM J. Math. Anal.*, **37** (2005), 598-618.
[12] S. N. Chandler-Wilde and J. Elschner, Variational approach in weighted Sobolev spaces to scattering by unbounded rough surfaces, *SIAM J. Math. Anal.*, **42** (2010), 2554-2580.
[13] J. Cheng, V. Isakov and S. Lu, Increasing stability in the inverse source problem with many frequencies, *J. Differential Equations*, **260** (2016), 4786-4804.
[14] D. Colton and R. Kress, *Inverse Acoustic and Electromagnetic Scattering Theory*, Applied Mathematical Sciences, vol. 93, Springer-Verlag, Berlin, 1998.
[15] A. S. Fokas, Y. Kurylev and V. Marinakis, The unique determination of neuronal currents in the brain via magnetoencephalography, *Inverse Problems*, **20** (2004), 1067-1082.
[16] G. Hu, X. Liu, F. Qu and B. Zhang, Variational approach to rough surface scattering problems with Neumann and generalized impedance boundary conditions, *Communications in Mathematical Sciences*, **13** (2015), 511-537.
[17] G. Hu, W. Lu and A. Rathsfeld, Acoustic scattering from locally perturbed periodic surfaces, *SIAM J. Appl. Math.*, **81** (2021), 2569-2595.
[18] V. Isakov and S. Lu, Increasing stability in the inverse source problem with attenuation and many frequencies, *SIAM J. Appl. Math.*, **78** (2018), 1-18.
[19] A. Kirsch, *An Introduction to the Mathematical Theory of Inverse Problems*, Applied Mathematical Sciences, vol. 120, Springer-Verlag, New York, 1996.
[20] A. Kirsch, A scattering problem for a local perturbation of an open periodic waveguide, *Math. Meth. Appl. Sci.*, **45** (2022), 5737-5773.
[21] J. Li, P. Li, H. Liu and X. Liu, Recovering multiscale buried anomalies in a two-layered medium, *Inverse Problems*, **31** (2015), 105006, 28 pp.
[22] P. Li, J. Wang and L. Zhang, Inverse obstacle scattering for Maxwell's equations in an unbounded structure, *Inverse Problems*, **35** (2019), 095002, 30 pp.
[23] P. Li and G. Yuan, Increasing stability for the inverse source scattering problem with multi-frequencies, *Inverse Problems Imaging*, **11** (2017), 745-759.
[24] P. Li, X. Yao and Y. Zhao, Stability for an inverse source problem of the biharmonic operator, *SIAM J. Appl. Math.*, **81** (2021), 2503-2525.
[25] P. Li, J. Zhai and Y. Zhao, Stability for the acoustic inverse source problem in inhomogeneous media, *SIAM J. Appl. Math.*, **80** (2020), 2547-2559.
[26] X. Liu and B. Zhang, A uniqueness result for the inverse electromagnetic scattering problem in a two-layered medium, *Inverse Problems*, **26** (2010), 105007, 11 pp.
[27] M. Thomas, *Analysis of Rough Surface Scattering Problems*, University of Reading, Reading: UK; 2006.
[28] J. Yang and K. Liu, Detecting buried wave-penetrable scatterers in a two-layered medium, *J. Comput. Appl. Math.*, **330** (2018), 318-329.
[29] Y. Zhang and X. Xu, Stability of a one-dimensional inverse source scattering problem in a multi-layered medium, *Inverse Problems and Imaging*, **17** (2023), 1113-1138.

[30] Y. Zhao, Stability for the electromagnetic inverse source problem in inhomogeneous media, *J. Inverse Ill-posed Problem*, **31** (2023), 103-116.

Received April 2023; revised September 2023; early access November 2023.